Mechanism of Void Nucleation and Growth in bcc Fe: Atomistic Simulations at Experimental Time Scales

Yue Fan, Akihiro Kushima, Sidney Yip, and Bilge Yildiz

Mechanism of Incipient Void Swelling in bcc-Fe: Atomistic Simulations at Experimental Time Scales

Yue Fan, Akihiro Kushima, Sidney Yip, and Bilge Yildiz[*]

Department of Nuclear Science and Engineering, Massachusetts Institute of Technology, 77

Massachusetts Avenue, Cambridge, Massachusetts, 02139, USA

---

[*] Corresponding author email: byildiz@mit.edu

Abstract

Evolution of small-vacancy clusters in bcc Fe is simulated using a multiscale approach coupling an atomistic activation-relaxation method for sampling transition-state pathways with environment-dependent reaction coordinate calculations and kinetic Monte Carlo simulation to reach time scales on the order of $\sim 10^4$ s. Under vacancy supersaturated condition, di- and tri-vacancy clusters form and grow by coalescence (Ostwald ripening). For cluster size greater than four we find a transition temperature of 150 ^{o}C for accelerated cluster growth, as observed in positron annihilation spectroscopy experiments. Implications for the mechanism of stage IV radiation damage recovery kinetics are discussed.

It is well known that the accumulation of radiation damage during microstructural evolution enhances the degradation of physical properties of structural materials owing to phenomena such as swelling, creep, and irradiation assisted cracking [1-3]. However, predicting irradiated microstructural and microchemical evolution over experimental times (seconds to years) has been a formidable challenge using conventional atomistic computational methods [4]; for example molecular dynamics (MD) can reach only up to nano-seconds. Rate theory [5, 6] and kinetic Monte Carlo (KMC) [7, 8] method have been used in the analysis of radiation damage accumulation, but they require input of atomistic details on defect interaction mechanisms and transition rates [9, 10] which in turn limits their predictive capability. This limitation is particularly serious in studies of defect evolution over long time scales, where the governing mechanisms are not known.

In this letter, we introduce a new approach to simulate defect structure evolution with atomistic fidelity capable of reaching experimental time scales (*hours*). We report results on early-phase void nucleation and growth mechanisms in bcc Fe with prediction of temperature variation of cluster size that can be matched to positron annihilation measurements probing the same process at the same spatial and temporal scales. Our approach begins with constructing the potential energy landscape and the associated atomic trajectories using a new activation-relaxation method of sampling transition state pathways, hereafter denoted as the Autonomous Basin Climbing (ABC) method [11-13]. We then compute the reaction barriers corresponding to the atomic trajectories by employing minimum energy path calculations [14] which connect the trajectories identified by ABC, and predict the governing

kinetics at relevant experimental time scales ($\sim 10^4$ s) according to transition state theory (TST) [15].

There are five generally accepted stages in radiation damage recovery process [16]. In bcc Fe, they are: stage I ($\sim$ -150 ^{o}C), migration of self-interstitial atoms (SIA); II ($\sim$ -100 ^{o}C), long range migration of SIA clusters; III ($\sim$ 0 ^{o}C), single vacancy migration; IV, migration of vacancy clusters; and stage V ($\sim$ 250 ^{o}C), thermal dissociation of vacancy clusters. The existence and dominant mechanism of stage IV have long been controversial [16-18], depending on material, impurities and irradiation conditions. In this work, our goal is to elucidate the conditions and the mechanism governing stage IV in pure bcc Fe, as this is the accelerating step in incipient void growth and swelling. We present atomistic details to show this transition stage (stage IV) is governed by the mobility and aggregation of small vacancy clusters of size less than ten vacancies, which match quantitatively with recent positron annihilation spectroscopy (PAS) experiments on neutron irradiated single crystal bcc Fe [19]. Our predicted transition temperature of 150 ^{o}C lies between stages III and V that was observed in the damage recovery upon electron irradiation [17]. These results indicate the existence of stage IV in bcc Fe under vacancy supersaturated conditions. The sizes of defects captured in our simulations are directly within the detection capability of the PAS technique in characterizing small vacancy clusters [19-23]. An implication of our work is the potential of the ABC algorithm to study atomistic mechanisms in long-term microstructural evolution in irradiated materials.

ABC is a method for sampling and reconstructing the system's potential energy surface (PES) developed recently by Kushima et al. [11] as an adaptation of the concept of metadynamics [24-26]. We have further extended this approach to study the unfaulting of self-trapped SIA clusters in bcc Fe [12] and thermal creep in bcc Fe [27]. Here, we consider the PES reconstruction in the formation and evolution of vacancy clusters. Starting with a minimum energy configuration with N atoms, an activation step is taken by adding a 3N dimensional Gaussian penalty function to the PES of the configuration. This is followed by a relaxation step of energy minimization where the added penalty pushes the system away from the initial configuration into a higher energy state. The cycle is repeated until the system crosses an energy saddle point during a relaxation step and enters into an adjacent potential energy well. This procedure enables the identification *without* prior knowledge of a transition-state pathway leading from one energy well to another, including the activation energy barrier and the atomic configurations. This feature of our method is not available in traditional rate theory and KMC simulations.

To gain computational efficiency in dealing with the early phase of vacancy agglomeration we find it useful to perform multiple simultaneous activations defined around each defect without restricting the defect-defect interactions in the entire system. Because the activations are applied individually, the barriers connecting the neighboring wells could be overestimated by ABC. To avoid this problem, we employ the nudged elastic band (NEB) method [14] to obtain more accurately the barriers between the neighboring energy minima identified by ABC. Thus ABC is used to find the reaction pathways, which are then assessed

by NEB to give the activation barriers. In turn the reaction pathways and barriers become input to KMC simulations of evolution kinetics of extended defects [28]. The transition rate between two states connected by barrier E is given by $k = k_0 \exp[-E / k_B T]$, where the jump frequency, k_0, is taken to be $5 \times 10^{12} s^{-1}$ in a first order approximation [28].

We use a cubic supercell with $10a_0 \times 10a_0 \times 10a_0$ dimensions for the ABC simulations. The system initially contains 50 randomly distributed single vacancies to represent a vacancy supersaturated structure in the central collision region after a displacement cascade [29] in single crystal bcc Fe. The embedded atom method (EAM) type potential developed by Ackland-Mendelev-Srolovitz (AMS) [30] is taken to be appropriate for the crystalline and the highly disordered phases relevant to our study. In the NEB calculations, 10 images are applied between each pair of initial and final states, and 229 successive minima states on the PES are explored. In the KMC simulations, as a first-order approximation, each energy minimum is connected only with its immediately preceding and following minima [10]. A total of 200 KMC simulations are performed to attain reliable statistics.

Fig.1 (a) shows the sequence of atomic configurations sampled by ABC with initial configuration C1. At the early phase (C2), the single vacancies migrate to combine with nearby vacancies to form small vacancy clusters. The di- and tri-vacancy clusters are able to migrate over longer distances, while clusters of size four and larger are less mobile and undergo only shape changes toward more stable configurations. In C3 and C4 the larger clusters grow by absorbing the mobile defects, particularly mono-vacancies and di- or

tri-vacancy clusters, while in C5 and C6 cluster growth is governed by aggregation of two less mobile clusters as discussed below and shown in Fig 1(b).
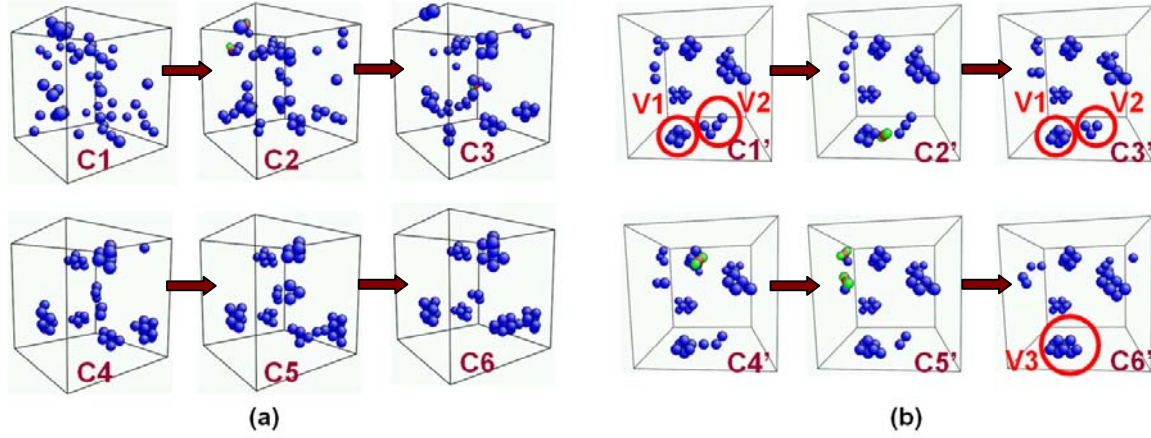

Figure 1. (Color Online) (a) Sequence of atomic configurations of vacancies in bcc Fe generated by ABC sampling (lattice atoms not shown) with initial configuration C1 consisting of 50 single vacancies. (b) Sequence of vacancy configurations depicting the reaction between two vacancy clusters, V1+V2 → V3. Blue balls represent the inserted vacancies, and red balls and green balls represent the interstitial atoms and vacant lattice sites, respectively, that arise during the vacancy cluster structure evolution.

Fig.1 (b) illustrates the interaction between two relatively immobile vacancy clusters of size 6 (V1) and 4 (V2), in which the smaller cluster dissociates by emitting one vacancy at a time, and the dissociated vacancies migrate toward V1. The process ends with V2 becoming a cluster of 10 vacancies and V1 disappearing. This is a demonstration of Ostwald ripening mechanism at the atomistic level [31].

In the simulations shown in Figure 1, the clusters range in size from a single vacancy to 16 vacancies. This range is ideally suitable for direct comparison with PAS measurements on temperature dependent size distribution of vacancy clusters [19, 20]. It has been observed in bcc Fe [19] that the number of clusters with 6 or fewer vacancies undergoes a sudden drop at

a temperature around 150 ℃, while correspondingly the number of larger vacancy clusters increases significantly. For the purpose of interpreting these results we focus on simulations in which the starting configuration had vacancy clusters of average size around 6 vacancies per cluster, consistent with the state at the beginning of the PAS measurements in Ref. 19. The potential energy landscape for the system evolution (exemplified in Fig. 1) is constructed by from 228 NEB calculations based on 229 successive minimum energy states explored by the ABC method. The resulting PES is shown in Fig. 2 (a). The average size of vacancy clusters is seen to increase from 6 to 9, while the system systematically evolves toward lower energy configurations.

On the basis of the energy landscape thus produced, the temperature and time dependence of the average cluster size are then obtained by KMC simulations. Using initial configurations (same as at the beginning of the PES in Fig. 2) which have an average cluster size of 6 the simulation is terminated when the average cluster size reaches 9. The initial temperature and annealing rate are set at 50 ℃ and 0.01 K/s, respectively, the conditions reported in the PAS experiments [19].
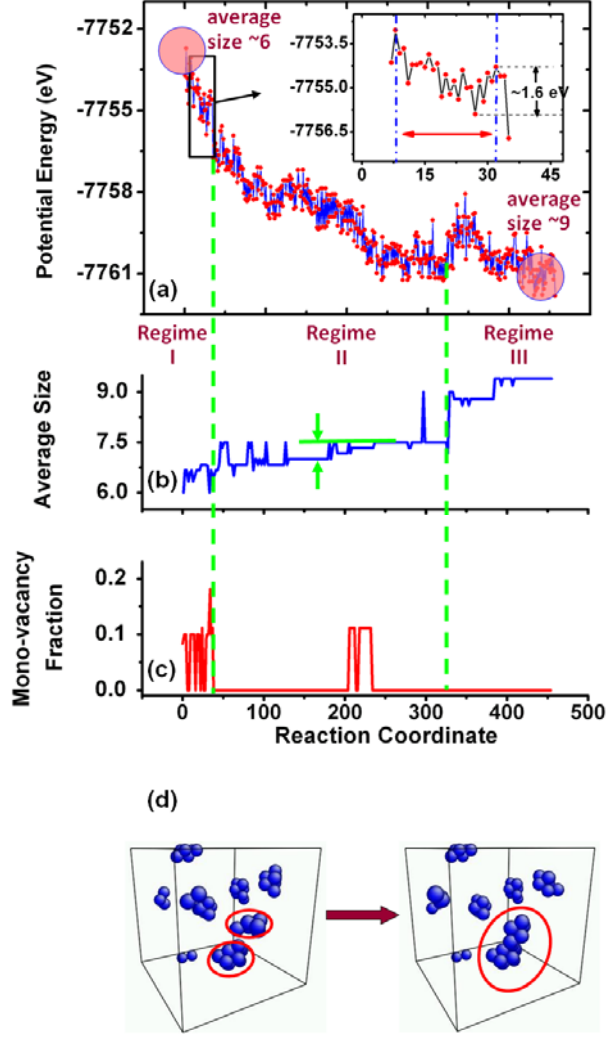
Figure 2. (Color Online) (a) The PES associated with a subset of the structural evolution shown in Figure 1(a), with initial and final average clusters of 6 and 9 vacancies, respectively. Inset: A region on the PES where the system is trapped in the early stages of evolution. (b) The average vacancy cluster size associated with the PES in (a). (c) Fraction of mono-vacancies among all the defects during structural evolution. (d) Evolution of vacancy clusters corresponding to the size increase seen in Regime III in (b).

Fig.3 shows the temperature variation of the average vacancy cluster size predicted by our KMC simulations over a time duration of about $2 \times 10^4 s$. Also shown are the intensity data from PAS experiments [19]. To compare the temperature dependence of cluster size prediction with intensity measurements, the two results are normalized (admittedly arbitrarily) at a temperature of ~120 ^{o}C in the middle of the plateau region. In the simulated results,

9

below 150 ℃ the clusters are stable and exhibit a slow increase in average size from 6 to 6.5. This is because the defect clusters are rather immobile and do not interact much with each other. In this temperature range the activated processes with low barriers are migration of mono-vacancies and shape change of vacancy clusters. From the potential energy landscape perspective the system is trapped in a local minimum and the thermal fluctuations are not sufficient to activate cluster evolution. This minimum is shown in the inset of Fig.2 (a). The entry barrier from left side into this region is lower than 1 eV, which makes the process feasible at low temperatures (< 150 ^{o}C). Once the system is in this region, however, further evolution forward or backward is hindered by high barriers. To evolve forward out of this minimum, the system needs to overcome an effective activation energy of around 1.6 eV, which implies a relatively high transition temperature or a nearly constant average cluster size below the transition temperature (see Regime I in Fig. 2 (b)). When the temperature exceeds 150℃, the system is able to overcome the forward barrier. At the same time at this temperature the remaining mono-vacancies disappear, as seen from the sudden drop of the red plot in Fig. 2 (c). Correspondingly cluster size begins to grow. The step from Regime II to III in Fig. 2 (b) is associated with the onset of the Ostwald ripening process discussed above. The spike in Fig. 2 (c) at reaction step 200 represents the re-appearance of mono-vacancies in the Ostwald ripening process (see Fig. 1 (b)). A significant increase of the average size occurs in the transition to Regime III. The governing mechanism here is the aggregation of two clusters (containing 6 and 10 vacancies, respectively) into a single cluster, as shown in Fig. 2 (d). The significantly larger standard deviation in the average size seen at 175-200 ^{o}C is consistent with the enhanced fluctuations expected in the transition
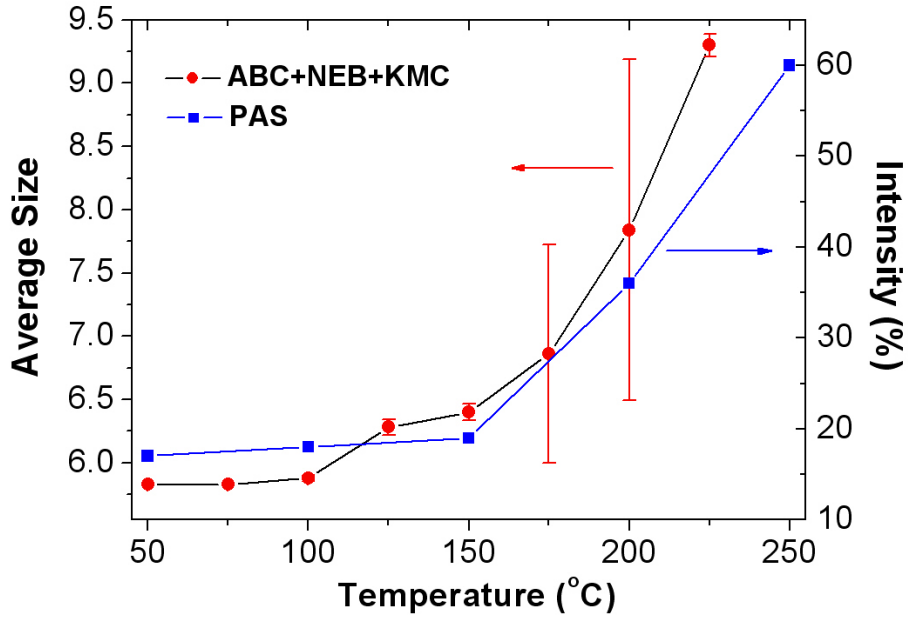
temperature range.

Figure 3. (Color Online) Temperature dependence of the average cluster size (red points) simulated by KMC based on the PES in Fig. 2(a), and the PAS data (blue points) [19] showing the relative intensity of vacancy clusters with size larger than ten.

We believe our finding demonstrates that 150 ℃ is a transition temperature for enabling the migration of vacancy clusters in a vacancy supersaturated bcc Fe that leads to their accumulation via the atomistic mechanisms demonstrated in Fig 1 (b) and Fig. 2 (d). This characteristic temperature therefore delineates the damage recovery stage IV, the existence of which has been controversial in the experimental literature. In the case of electron irradiated iron, only stages III (~ 0℃) and V (~ 250℃) were observed [17]. This is because only a low density of vacancies is produced upon electron irradiation, making cluster formation and survival difficult. In neutron irradiation it is possible to induce a supersaturation of vacancy defects, thus a higher probability to form clusters and survive up to higher temperatures [16]. Our simulation conditions and results correspond more closely to the latter.

While we have simulated a model bcc Fe system that was used in experiments, in real alloys impurities can be expected to significantly affect the defect reaction kinetics, and therefore warrant further studies. For example, the presence of C increases the vacancy migration barrier in bcc Fe [32] which could lead to an increase in the transition temperatures [17], and strong hydrogen-vacancy interactions are known to play an important role in determining the energetics and concentrations of point defect clusters [33]. In extending the present work to impurities, the ability of ABC to selectively activate a local region (down to one atom) should prove to be advantageous.

In conclusion, we have demonstrated a multiscale framework of combing ABC, NEB and KMC methods to elucidate the incipient evolution mechanisms in void swelling in irradiated bcc Fe, while retaining atomistic resolution. In our findings the vacancy clusters essentially do not grow between 50 and 150 $^{\circ}$C, while above the characteristic temperature of 150 ℃ accelerated growth occurs and is governed by cluster mobility and accumulation. The predicted critical temperature and cluster size are consistent with the PAS experiments. This agreement suggests a new interpretation, based on atomistic mechanisms, of damage recovery stage IV in bcc Fe. The broader implication of this work is that advances in multiscale modeling and simulation capabilities are beginning to enable quantitative, mechanistic analysis of suitable experiments on defect structure evolution.

References

[1] L. K. Mansur, Journal of Nuclear Materials **216**, 97 (1994).

[2] G. S. Was, Journal of Nuclear Materials **367-370**, 11 (2007).

[3] G. R. Odette *et al*, Annual Review of Materials Research **38**, 471 (2008).

[4] A. F. Voter *et al*, Annual Review of Materials Research **32**, 321 (2002).

[5] M. P. Surh *et al*, Journal of Nuclear Materials **328**, 107 (2004).

[6] G. R. Odette *et al*, Philos Mag **85**, 779 (2005).

[7] C. C. Fu *et al.*, Nat Mater **4**, 68 (2005).

[8] J. Marian *et al.*, Mat. Res. Soc. Symp. Proc. **650**, R3.2.1 (2001).

[9] M. Kabir *et al.*, Physical Review Letters **105**, 095501 (2010).

[10] See supplementary material for I) computed vacancy migration barriers as a function of distance from a void in bcc Fe; II) details of the KMC simulations implemented in this paper..

[11] A. Kushima *et al.*, The Journal of Chemical Physics **130**, 224504 (2009).

[12] Y. Fan *et al*, Physical Review B **81**, 104102 (2010).

[13] P. R. Monasterio, in *Ph.D. Thesis* (MIT, Cambridge, 2010).

[14] G. Henkelman *et al*, The Journal of Chemical Physics **113**, 9978 (2000).

[15] R. W. Zwanzig, *Nonequilibrium statistical mechanics* (Oxford university press, Oxford ; New York, 2001).

[16] W. Schilling *et al*, in Fundamental Aspects of Radiation Damage in Metals, Vol. I, CONF-751006-P1, edited by M. T. Robinson, and F. W. Young Oak Ridge, Tenn., (1975), p. 470.

[17] S. Takaki *et al.*, Radiat. Eff. **79**, 87 (1983).

[18] A. L. Nikolaev *et al.*, J Phys-Condens Mat **9**, 4385 (1997); A. L. Nikolaev *et al.*, Philos. Mag. **87**, 4847 (2007).

[19] M. Eldrup *et al*, Journal of Nuclear Materials **323**, 346 (2003).

[20] M. J. Puska *et al*, J Phys F Met Phys **13**, 333 (1983).

[21] J. Arponen *et al*, Ann Phys-New York **121**, 343 (1979).

[22] R. P. Gupta *et al*, J Phys F Met Phys **10**, L7 (1980).

[23] S. C. Glade *et al.*, Philos Mag **85**, 629 (2005).

[24] A. Laio *et al*, Proc Natl Acad Sci U S A **99**, 12562 (2002).

[25] A. Laio *et al*, Reports on Progress in Physics **71**, 126601 (2008).

[26] A. Barducci *et al*, Phys Rev Lett **100**, 020603 (2008).

[27] T. T. Lau *et al*, Physical Review Letters **104**, 175501 (2010).

[28] A. F. Voter, in *Radiation Effects in Solids* edited by K. E. Sickafus, E. A. Kotomin, and B. P. Uberuaga (Springer, Berlin, 2007), p. 1~24.

[29] D. J. Bacon *et al.*, Journal of Nuclear Materials **323**, 152 (2003).

[30] G. J. Ackland *et al.*, J Phys-Condens Mat **16**, S2629 (2004).

[31] R. W. Balluffi *et al.*, *Kinetics of materials* (J. Wiley & Sons, Hoboken, N.J., 2005).

[32] T. T. Lau *et al.*, Phys Rev Lett **98**, 215501 (2007).

[33] P. R. Monasterio *et al.*, Phys Rev Lett **103**, 085501 (2009).